



# A sampling surfaces method and its implementation for 3D thermal stress analysis of functionally graded plates



G.M. Kulikov\*, S.V. Plotnikova

Department of Applied Mathematics and Mechanics, Tambov State Technical University, Sovetskaya Street, 106, Tambov 392000, Russia

## ARTICLE INFO

Article history:  
Available online 20 October 2014

Keywords:  
Thermoelasticity  
Functionally graded plate  
3D stress analysis  
Sampling surfaces method

## ABSTRACT

The paper deals with a recently developed method of sampling surfaces (SaS) and its implementation for the three-dimensional (3D) steady-state problem of thermoelasticity for laminated functionally graded (FG) plates subjected to thermomechanical loading. The SaS method is based on choosing inside the  $n$ th layer  $I_n$  not equally spaced SaS parallel to the middle surface of the plate in order to introduce temperatures and displacements of these surfaces as basic plate variables. Such an idea permits the presentation of the thermoelastic laminated FG plate formulation in a very compact form. The SaS are located inside each layer at Chebyshev polynomial nodes that provides a uniform convergence of the SaS method. This means that the SaS method can be applied efficiently to the 3D stress analysis for thermoelastic laminated FG plates with a specified accuracy utilizing the sufficient number of SaS.

© 2014 Elsevier Ltd. All rights reserved.

## 1. Introduction

Nowadays, the functionally graded (FG) materials are widely used in mechanical engineering due to their advantages compared to traditional laminated materials [1,2]. However, the study of FG materials is not a simple task because the material properties depend on the spatial coordinate and some specific assumptions regarding their continuous variations in the thickness direction are required [3]. This fact restricts the implementation of the Pagano approach [4,5] and the state space approach [6,7] for the 3D exact analysis of FG simply supported rectangular plates. Another popular approach to 3D exact solutions, namely, asymptotic approach was applied efficiently to FG plates subjected to thermomechanical loading [8,9]. A new approach to closed-form elasticity solutions for FG isotropic and transversely isotropic plates is considered in papers [10,11]. These solutions are based on the general solution of the equilibrium equations of inhomogeneous elastic media [12]. The efficient approach to the 3D exact analysis of thermoelasticity has been proposed by Vel and Batra [13,14]. They studied the static and transient thermoelastic problems for FG simply supported plates with the material properties presented by Taylor series expansions through the thickness coordinate. Ootao and his coauthors [15–17] obtained the 3D exact solutions for the transient thermoelastic response of FG strips and rectangular plates with simply supported edges under nonuniform heating

on outer surfaces. The original approach to analytical solutions for the FG beams and plates was developed in contributions [18,19]. This approach is based on the so-called theory of directed surfaces [20,21]. Recently, the sampling surfaces (SaS) approach has been applied to 3D exact thermal and thermoelastic analyses of laminated composite plates and shells [22–24]. The 3D stress analysis of piezoelectric FG plates and shells on the basis of the SaS method is given in [25,26]. However, the SaS approach has not been applied to 3D steady-state thermoelasticity problems for laminated FG plates yet.

According to the SaS method [27,28], we choose inside the  $n$ th layer  $I_n$  not equally spaced SaS  $\Omega^{(n)1}, \Omega^{(n)2}, \dots, \Omega^{(n)I_n}$  parallel to the middle surface of the plate and introduce temperatures  $T^{(n)1}, T^{(n)2}, \dots, T^{(n)I_n}$  and displacement vectors  $\mathbf{u}^{(n)1}, \mathbf{u}^{(n)2}, \dots, \mathbf{u}^{(n)I_n}$  of these surfaces as basic plate variables, where  $I_n \geq 3$ . Such choice of unknowns in conjunction with the use of the Lagrange polynomials of degree  $I_n - 1$  in the thickness direction permits the presentation of governing equations of the proposed thermoelastic FG plate formulation in a very compact form.

It should be mentioned that the SaS method with equally spaced SaS does not work properly with the Lagrange polynomials of high degree because of the Runge's phenomenon [29]. This phenomenon can yield the wild oscillation at the edges of the interval when the user deals with any specific functions. If the number of equally spaced nodes is increased then the oscillations become even larger. However, the use of the Chebyshev polynomial nodes [30] inside each layer can help to improve significantly the behavior of the Lagrange polynomials of high degree because such a

\* Corresponding author.

E-mail address: [gmkulikov@mail.ru](mailto:gmkulikov@mail.ru) (G.M. Kulikov).

choice allows one to minimize uniformly the error due to the Lagrange interpolation.

Currently, the use of layer-wise theories for the analysis of laminated composite plates is widely accepted. The most general form of layer-wise kinematics presented in Carrera’s unified formulation [31] is written as

$$u_i^{(n)} = F_0 u_i^{[n-1]} + F_1 u_i^{[n]} + \sum_r F_r u_{ir}^{(n)}, \quad x_3^{[n-1]} \leq x_3 \leq x_3^{[n]},$$

$$F_0(x_3) = \frac{x_3^{[n]} - x_3}{h_n}, \quad F_1(x_3) = \frac{x_3 - x_3^{[n-1]}}{h_n}, \quad F_r(x_3^{[n-1]}) = F_r(x_3^{[n]}) = 0,$$

where  $u_i^{(n)}(x_1, x_2, x_3)$  are the displacements of the  $n$ th layer ( $i = 1, 2, 3$ );  $u_i^{[n-1]}(x_1, x_2)$  and  $u_i^{[n]}(x_1, x_2)$  are the displacements of the bottom and top surfaces of the  $n$ th layer (interfaces);  $u_{ir}^{(n)}(x_1, x_2)$  are the generalized displacements of the  $n$ th layer ( $r = 2, 3, \dots, R$ );  $F_r(x_3)$  are the prescribed polynomials of degree  $r$ ;  $x_3^{[n-1]}$  and  $x_3^{[n]}$  are the transverse coordinates of layer interfaces  $\Omega^{[n-1]}$  and  $\Omega^{[n]}$  (Fig. 1);  $h_n = x_3^{[n]} - x_3^{[n-1]}$  is the thickness of the  $n$ th layer;  $x_1$  and  $x_2$  are the Cartesian coordinates of the middle surface  $\Omega$ ;  $x_3$  is the thickness coordinate normal to the middle surface; the index  $n$  identifies the belonging of any quantity to the  $n$ th layer and runs from 1 to  $N$ , where  $N$  is the number of layers. Historically, the first order layer-wise models [32–35] were first. Then, the second order models with  $R = 2$  and third order models with  $R = 3$  were developed [36–38]. The fourth order layer-wise model ( $R = 4$ ) is utilized in Carrera’s unified formulation [39–41], where polynomials  $F_r$  are evaluated as a difference between two Legendre polynomials of degrees  $r$  and  $r - 2$ .

The origins of using the SaS can be found in contributions [42,43] in which three, four and five equally spaced SaS are employed. The SaS method with the arbitrary number of equispaced SaS is considered in [44]. The more general approach with the SaS located at Chebyshev polynomial nodes has been developed later [27,28]. Note also that the term SaS should not be confused with such terms as a mathematical surface or a virtual surface, which are extensively utilized in Carrera’s unified formulation. This is due to the fact that in Carrera’s unified formulation the generalized displacements of layers  $u_{ir}^{(n)}$  are employed. On the contrary, in a developed SaS formulation all basic variables have a clear mechanical sense because of the introduction of temperatures and displacements of SaS as plate unknowns. The similar technique is adopted for the description of material properties, which are also referred to SaS. This gives the opportunity to derive the 3D exact solutions for laminated FG plates with a prescribed accuracy utilizing the sufficiently large number of SaS located at Chebyshev polynomial nodes inside each layer. Furthermore, in a

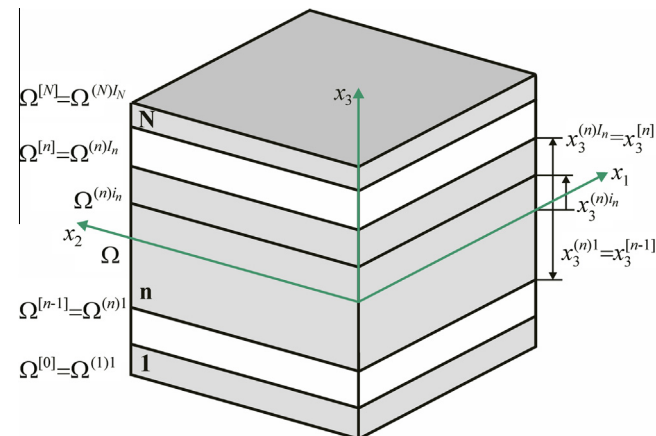


Fig. 1. Geometry of the laminated plate.

SaS formulation for shells such choice of displacements as fundamental unknowns yields the strain–displacement equations, which exactly represent rigid-body motions of the shell in any convected curvilinear coordinate system [28]. The latter is straightforward for development of the exact geometry solid-shell elements [45,46]. The term “exact geometry” reflects the fact that the parametrization of the middle surface is known and, therefore, the coefficients of the first and second fundamental forms of its surface can be taken exactly at each element node.

## 2. Description of temperature and temperature gradient fields

Consider a laminated FG plate of the thickness  $h$ . The transverse coordinates of SaS of the  $n$ th layer are defined as

$$x_3^{(n)1} = x_3^{[n-1]}, \quad x_3^{(n)l_n} = x_3^{[n]},$$

$$x_3^{(n)m_n} = \frac{1}{2} \left( x_3^{[n-1]} + x_3^{[n]} \right) - \frac{1}{2} h_n \cos \left( \pi \frac{2m_n - 3}{2(I_n - 2)} \right), \quad (1)$$

where  $l_n$  is the number of SaS corresponding to the  $n$ th layer; the index  $m_n$  identifies the belonging of any quantity to the inner SaS of the  $n$ th layer and runs from 2 to  $l_n - 1$ , whereas the indices  $i_n, j_n, k_n$  to be introduced later for describing all SaS of the  $n$ th layer run from 1 to  $l_n$ . Besides, the tensorial indices  $i, j, k, l$  range from 1 to 3 and Greek indices  $\alpha, \beta$  range from 1 to 2.

**Remark 1.** The transverse coordinates of inner SaS (1) coincide with coordinates of the Chebyshev polynomial nodes [30]. This fact has a great meaning for a convergence of the SaS method [22–28].

The relation between the temperature  $T$  and the temperature gradient  $\Gamma$  is given by

$$\Gamma = \nabla T. \quad (2)$$

In a component form, it can be written as

$$\Gamma_i = T_{,i}, \quad (3)$$

where the symbol  $(\dots)_{,i}$  stands for the partial derivatives with respect to coordinates  $x_i$ .

We start now with the first and second fundamental assumptions of the proposed thermoelastic laminated plate formulation. Let us assume that the temperature and temperature gradient fields are distributed through the thickness of the  $n$ th layer as follows:

$$T^{(n)} = \sum_{i_n} L^{(n)i_n} T^{(n)i_n}, \quad x_3^{[n-1]} \leq x_3 \leq x_3^{[n]}, \quad (4)$$

$$\Gamma_i^{(n)} = \sum_{i_n} L^{(n)i_n} \Gamma_i^{(n)i_n}, \quad x_3^{[n-1]} \leq x_3 \leq x_3^{[n]}, \quad (5)$$

where  $T^{(n)i_n}(x_1, x_2)$  are the temperatures of SaS of the  $n$ th layer  $\Omega^{(n)i_n}$ ;  $\Gamma_i^{(n)i_n}(x_1, x_2)$  are the components of the temperature gradient at the same SaS;  $L^{(n)i_n}(x_3)$  are the Lagrange polynomials of degree  $l_n - 1$  defined as

$$T^{(n)i_n} = T(x_3^{(n)i_n}), \quad (6)$$

$$\Gamma_i^{(n)i_n} = \Gamma_i(x_3^{(n)i_n}), \quad (7)$$

$$L^{(n)i_n} = \prod_{j_n \neq i_n} \frac{x_3 - x_3^{(n)j_n}}{x_3^{(n)i_n} - x_3^{(n)j_n}}. \quad (8)$$

The use of Eqs. (3), (4), (6) and (7) yields

$$\Gamma_{\alpha}^{(n)i_n} = T_{,\alpha}^{(n)i_n}, \quad (9)$$

$$\Gamma_3^{(n)i_n} = \sum_{j_n} M^{(n)j_n} \left( x_3^{(n)j_n} \right) T^{(n)j_n}, \quad (10)$$

where  $M^{(n)j_n} = L_3^{(n)j_n}$  are the derivatives of the Lagrange polynomials, which are calculated at SaS as follows:

$$M^{(n)j_n} \left( x_3^{(n)i_n} \right) = \frac{1}{x_3^{(n)j_n} - x_3^{(n)i_n}} \prod_{k_n \neq i_n, j_n} \frac{x_3^{(n)j_n} - x_3^{(n)k_n}}{x_3^{(n)j_n} - x_3^{(n)k_n}} \text{ for } j_n \neq i_n, \\ M^{(n)i_n} \left( x_3^{(n)i_n} \right) = - \sum_{j_n \neq i_n} M^{(n)j_n} \left( x_3^{(n)i_n} \right). \quad (11)$$

It is seen from Eq. (10) that the transverse component of the temperature gradient  $\Gamma_3^{(n)i_n}$  is represented as a linear combination of temperatures of all SaS of the  $n$ th layer  $T^{(n)j_n}$ .

### 3. Description of displacement and strain fields

The strain components  $\varepsilon_{ij}$  are written as

$$2\varepsilon_{ij} = u_{i,j} + u_{j,i}, \quad (12)$$

where  $u_i$  are the displacements of the plate.

Following the SaS technique, we introduce the third and fourth assumptions of the thermoelastic laminated FG plate formulation. Let us assume that displacement and strain distributions through the thickness of the  $n$ th layer are similar to thermal and temperature gradient distributions (4) and (5), that is

$$u_i^{(n)} = \sum_{i_n} L^{(n)i_n} u_i^{(n)i_n}, \quad x_3^{[n-1]} \leq x_3 \leq x_3^{[n]}, \quad (13)$$

$$\varepsilon_{ij}^{(n)} = \sum_{i_n} L^{(n)i_n} \varepsilon_{ij}^{(n)i_n}, \quad x_3^{[n-1]} \leq x_3 \leq x_3^{[n]}, \quad (14)$$

where  $u_i^{(n)i_n}(x_1, x_2)$  are the displacements of SaS  $\Omega^{(n)i_n}$ ;  $\varepsilon_{ij}^{(n)i_n}(x_1, x_2)$  are the strains of the same SaS defined as

$$u_i^{(n)i_n} = u_i \left( x_3^{(n)i_n} \right), \quad (15)$$

$$\varepsilon_{ij}^{(n)i_n} = \varepsilon_{ij} \left( x_3^{(n)i_n} \right). \quad (16)$$

Using Eqs. (12), (13), (15) and (16), one obtains

$$2\varepsilon_{\alpha\beta}^{(n)i_n} = u_{\alpha,\beta}^{(n)i_n} + u_{\beta,\alpha}^{(n)i_n}, \quad (17)$$

$$2\varepsilon_{23}^{(n)i_n} = \beta_{\alpha}^{(n)i_n} + u_{3,\alpha}^{(n)i_n}, \quad (18)$$

$$\varepsilon_{33}^{(n)i_n} = \beta_3^{(n)i_n}, \quad (19)$$

$$\beta_i^{(n)i_n} = u_{i,3} \left( x_3^{(n)i_n} \right), \quad (20)$$

where  $\beta_i^{(n)i_n}(x_1, x_2)$  are the values of derivatives of displacements with respect to thickness coordinate  $x_3$  at SaS defined as

$$\beta_i^{(n)i_n} = \sum_{j_n} M^{(n)j_n} \left( x_3^{(n)i_n} \right) u_i^{(n)j_n}. \quad (21)$$

This means that the key functions  $\beta_i^{(n)i_n}$  of the proposed thermoelastic laminated plate formulation are represented as a linear combination of displacements of SaS of the  $n$ th layer  $u_i^{(n)j_n}$ .

### 4. Variational formulation of heat conduction problem

The variational equation for the thermal laminated plate can be written as

$$\delta J = 0, \quad (22)$$

where  $J$  is the basic functional of the heat conduction theory given by

$$J = \frac{1}{2} \iint_{\Omega} \sum_n \int_{x_3^{[n-1]}}^{x_3^{[n]}} q_i^{(n)} \Gamma_i^{(n)} dx_1 dx_2 dx_3 - \iint_{\Omega} T Q_n d\Omega, \quad (23)$$

where  $q_i^{(n)}$  are the components of the heat flux vector of the  $n$ th layer;  $Q_n$  is the specified heat flux on the boundary surface

$\bar{\Omega} = \Omega^{[0]} + \Omega^{[N]} + \Sigma$ , where  $\Sigma$  is the edge boundary surface of the plate. Here and in the following developments, the summation on repeated Latin indices is implied.

Substituting the through-thickness distribution (5) in Eq. (23) and introducing heat flux resultants

$$R_i^{(n)i_n} = \int_{x_3^{[n-1]}}^{x_3^{[n]}} q_i^{(n)} L^{(n)i_n} dx_3, \quad (24)$$

one obtains

$$J = \frac{1}{2} \iint_{\Omega} \sum_n \sum_{i_n} R_i^{(n)i_n} \Gamma_i^{(n)i_n} dx_1 dx_2 - \iint_{\Omega} T Q_n d\Omega. \quad (25)$$

The Fourier's heat conduction equations are expressed as follows:

$$q_i^{(n)} = -k_{ij}^{(n)} \Gamma_j^{(n)}, \quad x_3^{[n-1]} \leq x_3 \leq x_3^{[n]}, \quad (26)$$

where  $k_{ij}^{(n)}$  are the components of the thermal conductivity tensor of the  $n$ th layer.

Next, we accept the fifth assumption of the thermoelastic FG plate formulation. Let us assume that thermal conductivity coefficients of the  $n$ th layer are distributed through the thickness of a plate according to the following law:

$$k_{ij}^{(n)} = \sum_{i_n} L^{(n)i_n} k_{ij}^{(n)i_n}, \quad (27)$$

that is extensively utilized in this paper, where  $k_{ij}^{(n)i_n}$  are the values of the thermal conductivity coefficients on SaS of the  $n$ th layer.

The use of Eqs. (5), (26) and (27) into Eq. (24) leads to

$$R_i^{(n)i_n} = - \sum_{j_n, k_n} \Lambda^{(n)i_n j_n k_n} k_{ij}^{(n)j_n} \Gamma_j^{(n)k_n}, \quad (28)$$

where

$$\Lambda^{(n)i_n j_n k_n} = \int_{x_3^{[n-1]}}^{x_3^{[n]}} L^{(n)i_n} L^{(n)j_n} L^{(n)k_n} dx_3. \quad (29)$$

### 5. Variational formulation of thermoelastic plate problem

The variational equation for the thermoelastic laminated plate in the case of conservative loading can be written as [47]

$$\delta \Pi = 0, \quad (30)$$

where

$$\Pi = \iint_{\Omega} \sum_n \int_{x_3^{[n-1]}}^{x_3^{[n]}} F^{(n)} dx_1 dx_2 dx_3 - W, \quad (31)$$

$$F^{(n)} = \frac{1}{2} \left( \sigma_{ij}^{(n)} \varepsilon_{ij}^{(n)} - \eta^{(n)} \Theta^{(n)} \right), \quad (32)$$

$$W = \iint_{\Omega} \left( p_i^+ u_i^{[N]} - p_i^- u_i^{[0]} \right) dx_1 dx_2 + W_{\Sigma}, \quad (33)$$

where  $F^{(n)}$  is the free-energy density of the  $n$ th layer;  $\sigma_{ij}^{(n)}$  are the components of the stress tensor of the  $n$ th layer;  $\eta^{(n)}$  is the entropy density of the  $n$ th layer;  $u_i^{[0]} = u_i^{(1)1}$  and  $u_i^{[N]} = u_i^{(N)N}$  are the displacements of the bottom and top surfaces  $\Omega^{[0]}$  and  $\Omega^{[N]}$ ;  $p_i^-$  and  $p_i^+$  are the loads acting on the bottom and top surfaces;  $W_{\Sigma}$  is the work done by external loads applied to the edge surface  $\Sigma$ ;  $\Theta^{(n)}$  is the temperature rise from the initial reference temperature  $T_0$  defined as

$$\Theta^{(n)} = T^{(n)} - T_0. \quad (34)$$

Substituting the strain distribution (14) and temperature distribution

$$\Theta^{(n)} = \sum_{i_n} L^{(n)i_n} \Theta^{(n)i_n}, \quad x_3^{[n-1]} \leq x_3 \leq x_3^{[n]}, \quad (35)$$

which follows from Eqs. (4) and (34) into Eqs. (31) and (32), and introducing stress resultants

$$H_{ij}^{(n)in} = \int_{x_3^{[n-1]}}^{x_3^{[n]}} \sigma_{ij}^{(n)} L^{(n)in} dx_3 \tag{36}$$

and entropy resultants

$$S^{(n)in} = \int_{x_3^{[n-1]}}^{x_3^{[n]}} \eta^{(n)} L^{(n)in} dx_3, \tag{37}$$

one obtains

$$\Pi = \frac{1}{2} \iint_{\Omega} \sum_n \sum_{i_n} \left( H_{ij}^{(n)in} \epsilon_{ij}^{(n)in} - S^{(n)in} \Theta^{(n)in} \right) dx_1 dx_2 - W. \tag{38}$$

For simplicity, we consider the case of linear thermoelastic materials [47], which are described by

$$\sigma_{ij}^{(n)} = C_{ijkl}^{(n)} \epsilon_{kl}^{(n)} - \gamma_{ij}^{(n)} \Theta^{(n)}, \quad x_3^{[n-1]} \leq x_3 \leq x_3^{[n]}, \tag{39}$$

$$\eta^{(n)} = \gamma_{ij}^{(n)} \epsilon_{ij}^{(n)} + \chi^{(n)} \Theta^{(n)}, \quad x_3^{[n-1]} \leq x_3 \leq x_3^{[n]}, \tag{40}$$

where  $C_{ijkl}^{(n)}$  are the elastic constants of the  $n$ th layer;  $\gamma_{ij}^{(n)}$  are the thermal stress coefficients of the  $n$ th layer;  $\chi^{(n)}$  is the entropy-temperature coefficient defined as

$$\chi^{(n)} = \rho^{(n)} c_v^{(n)} / T_0, \tag{41}$$

where  $\rho^{(n)}$  is the mass density of the  $n$ th layer;  $c_v^{(n)}$  is the specific heat per unit mass of the  $n$ th layer at constant strain.

Finally, we introduce the sixth assumption of the thermoelastic FG plate formulation. Let the material constants be distributed through the thickness of the plate as accepted throughout the paper

$$C_{ijkl}^{(n)} = \sum_{i_n} L^{(n)in} C_{ijkl}^{(n)in}, \tag{42}$$

$$\gamma_{ij}^{(n)} = \sum_{i_n} L^{(n)in} \gamma_{ij}^{(n)in}, \tag{43}$$

$$\chi^{(n)} = \sum_{i_n} L^{(n)in} \chi^{(n)in}, \tag{44}$$

where  $C_{ijkl}^{(n)in}$ ,  $\gamma_{ij}^{(n)in}$  and  $\chi^{(n)in}$  are the values of material constants on SaS of the  $n$ th layer.

Substituting constitutive equations (39) and (40) respectively into Eqs. (36) and (37) and taking into account the through-thickness distributions (14), (35), (42), (43) and (44), we arrive at final formulas for stress and entropy resultants

$$H_{ij}^{(n)in} = \sum_{j_n, k_n} \Lambda^{(n)inj_n k_n} \left( C_{ijkl}^{(n)in} \epsilon_{kl}^{(n)k_n} - \gamma_{ij}^{(n)in} \Theta^{(n)k_n} \right), \tag{45}$$

$$S^{(n)in} = \sum_{j_n, k_n} \Lambda^{(n)inj_n k_n} \left( \gamma_{kl}^{(n)in} \epsilon_{kl}^{(n)k_n} + \chi^{(n)in} \Theta^{(n)k_n} \right). \tag{46}$$

Here, coefficients  $\Lambda^{(n)inj_n k_n}$  are defined by Eq. (29).

### 6. Analytical solution for laminated FG rectangular plates

In this section, we study a laminated orthotropic rectangular plate subjected to thermomechanical loading. The boundary conditions for the simply supported plate with edges maintained at the reference temperature can be written as

$$\begin{aligned} \sigma_{11}^{(n)} = u_2^{(n)} = u_3^{(n)} = \Theta^{(n)} = 0 \quad \text{at } x_1 = 0 \text{ and } x_1 = a, \\ \sigma_{22}^{(n)} = u_1^{(n)} = u_3^{(n)} = \Theta^{(n)} = 0 \quad \text{at } x_2 = 0 \text{ and } x_2 = b, \end{aligned} \tag{47}$$

where  $a$  and  $b$  are the plate dimensions. To satisfy boundary conditions, we search for the analytical solution of the problem by a method of the double Fourier series expansion

$$\Theta^{(n)in} = \sum_{r,s} \Theta_{rs}^{(n)in} \sin \frac{r\pi x_1}{a} \sin \frac{s\pi x_2}{b}, \tag{48}$$

$$u_1^{(n)in} = \sum_{r,s} u_{1rs}^{(n)in} \cos \frac{r\pi x_1}{a} \sin \frac{s\pi x_2}{b}, \tag{49}$$

$$u_2^{(n)in} = \sum_{r,s} u_{2rs}^{(n)in} \sin \frac{r\pi x_1}{a} \cos \frac{s\pi x_2}{b},$$

$$u_3^{(n)in} = \sum_{r,s} u_{3rs}^{(n)in} \sin \frac{r\pi x_1}{a} \sin \frac{s\pi x_2}{b}, \tag{50}$$

where  $r$  and  $s$  are the wave numbers in plane directions. The external mechanical loads are also expanded in double Fourier series.

Substituting Fourier series (48) in Eqs. (9), (10), (25) and (28), and taking into account (34) and (35), one derives

$$J = \sum_{r,s} J_{rs} \left( \Theta_{rs}^{(n)in} \right). \tag{51}$$

Invoking the variational equation (22) and (51), we arrive at the system of linear algebraic equations

$$\frac{\partial J_{rs}}{\partial \Theta_{rs}^{(n)in}} = 0 \tag{52}$$

of order  $K$ , where  $K = \sum_n I_n - N + 1$ . Thus, the temperature rises of SaS of the  $n$ th layer  $\Theta_{rs}^{(n)in}$  can be found by using a method of Gaussian elimination.

Substituting next Fourier series (48)–(50), and Fourier series corresponding to mechanical loading in Eqs. (17), (18), (19), (21), (33), (38), (45) and (46), we obtain

$$\Pi = \sum_{r,s} \Pi_{rs} \left( u_{irs}^{(n)in}, \Theta_{rs}^{(n)in} \right). \tag{53}$$

The use of the variational equation (30) and (53) yields a system of linear algebraic equations

$$\frac{\partial \Pi_{rs}}{\partial u_{irs}^{(n)in}} = 0 \tag{54}$$

of order  $3K$ . Therefore, the displacements of SaS of the  $n$ th layer  $u_{irs}^{(n)in}$  can be found using again a method of Gaussian elimination.

The described algorithm was performed with the Symbolic Math Toolbox, which incorporates symbolic computations into

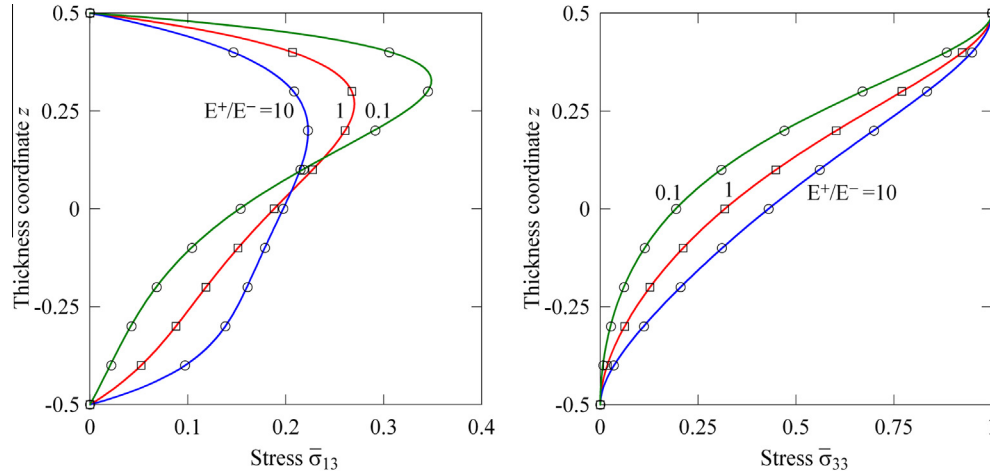
**Table 1**  
Results for a single-layer square plate with  $a/h = 3$  and  $\alpha = 0$ .

$I_1$	$-\bar{u}_1(0.5)$	$\bar{u}_3(0)$	$\bar{\sigma}_{11}(0.5)$	$-\bar{\sigma}_{12}(0.5)$	$\bar{\sigma}_{13}(0)$	$\bar{\sigma}_{33}(0)$
3	0.3986372494504680	1.278878243389591	1.999302146854837	0.8349039028805547	0.4977436151168003	0.4752837277628003
7	0.4358933937131948	1.342554953466513	2.124032428288413	0.9129329889584641	0.7022762666060094	0.4943950643281928
11	0.4358933942603120	1.342554689543095	2.124018410314048	0.9129329901043438	0.7023022083223538	0.4944039935419638
15	0.4358933942603121	1.342554689542491	2.124018410193782	0.9129329901043439	0.7023022084767580	0.4944039936052152
19	0.4358933942603120	1.342554689542491	2.124018410193780	0.9129329901043437	0.7023022084767578	0.4944039936052150
Exact [4] <sup>a</sup>	0.4358933942603120	1.342554689542491	2.124018410193781	0.9129329901043437	0.7023022084767578	0.4944039936052149

<sup>a</sup> The exact results have been obtained by the authors using the Vlasov's closed-form solution.

**Table 2**Results for a single-layer square plate with  $a/h = 3$  and  $\alpha = 0.1$ .

$I_1$	$-\bar{u}_1(0.5)$	$\bar{u}_3(0)$	$\bar{\sigma}_{11}(0.5)$	$-\bar{\sigma}_{12}(0.5)$	$\bar{\sigma}_{13}(0)$	$\bar{\sigma}_{33}(0)$
3	0.4158336502652652	1.347977241257294	2.073239906807475	0.8700097684529745	0.4983226799021384	0.4596565434470269
7	0.4536977979133792	1.414636043682728	2.193265858989844	0.9502222750248108	0.7020700339720654	0.4877173446168515
11	0.4536977984142576	1.414635771310962	2.193270258459039	0.9502224469642998	0.7020957676355946	0.4877129579452970
15	0.4536977984142576	1.414635771310368	2.193270258650021	0.9502224469653965	0.7020957677904856	0.4877129578319663
19	0.4536977984142575	1.414635771310368	2.193270258650021	0.9502224469653963	0.7020957677904854	0.4877129578319657
Exact [10]		1.41464				

**Fig. 2.** Through-thickness distributions of transverse stresses for a single-layer FG plate with  $a/h = 1$ : SaS formulation (-) for  $I_1 = 11$  and closed-form solutions [4] ( $\square$ ) and [10] ( $\circ$ ).

```

% Number of Sampling Surfaces In
% Calculation of Transverse Coordinates of Sampling Surfaces
for i=1:Ln
    theta_three(ln-i+1)=cos(pi*(2*i-1)/2/ln)*h/2;
end
% Calculation of Lagrange Polynomials
for i=1:Ln
    for j=1:Ln
        if(i~=j)
            L(i)=L(i)*(theta3-theta_three(j))/(theta_three(i)-theta_three(j));
        end
    end
end
% Calculation of Derivatives of Lagrange Polynomials
for i=1:Ln
    M(i)=diff(L(i),theta3);
end

```

**Fig. 3.** MATLAB module for calculating Lagrange polynomials and their derivatives.

the numeric environment of MATLAB. This gives an opportunity to obtain analytical solutions for laminated FG rectangular plates with a specified accuracy employing the sufficient number of SaS.

### 6.1. Single-layer FG square plate under mechanical loading

Consider a single-layer isotropic square plate subjected to transverse sinusoidal loading acting on its top surface

$$p_3^+ = p_0 \sin \frac{\pi x_1}{a} \sin \frac{\pi x_2}{b}, \quad p_3^- = 0, \quad (55)$$

where  $p_0 = 1$  Pa and  $a = b = 1$  m.

It is assumed that the elastic modulus is distributed in the thickness direction according to the exponential law

```

% Calculation of Loads
p3plus=p0*sin(pi*theta1/a)*sin(pi*theta2/b);
% Calculation of Displacements of Sampling Surfaces
for i=1:Ln
    u1(i)=U(i)*cos(pi*theta1/a)*sin(pi*theta2/b);
    u2(i)=U(ln+i)*sin(pi*theta1/a)*cos(pi*theta2/b);
    u3(i)=U(2*ln+i)*sin(pi*theta1/a)*sin(pi*theta2/b);
end
% Calculation of Strains of Sampling Surfaces
for i=1:Ln
    beta1(i)=sym('0');
    beta2(i)=sym('0');
    beta3(i)=sym('0');
end
for i=1:Ln
    for j=1:Ln
        beta1(i)=beta1(i)+subs(M(j),theta_three(i))*u1(j);
        beta2(i)=beta2(i)+subs(M(j),theta_three(i))*u2(j);
        beta3(i)=beta3(i)+subs(M(j),theta_three(i))*u3(j);
    end
end
for i=1:Ln
    eps11(i)=diff(u1(i),theta1);
    eps22(i)=diff(u2(i),theta2);
    eps33(i)=beta3(i);
    eps12(i)=(diff(u1(i),theta2)+diff(u2(i),theta1))/2;
    eps13(i)=(beta1(i)+diff(u3(i),theta1))/2;
    eps23(i)=(beta2(i)+diff(u3(i),theta2))/2;
end

```

**Fig. 4.** MATLAB module for calculating displacements and strains of sampling surfaces.

$$E = E^+ e^{\gamma(z-0.5)}, \quad z = x_3/h, \quad (56)$$

where  $E^+$  is the elastic modulus on the top surface;  $\gamma$  is the material gradient index defined as

```

% Calculation of Total Potential Energy
% Stress Resultants H11(i), H22(i), H33(i), H12(i), H13(i), H23(i)
Energy=sym('0');
for i=1:Ln
    Energy=Energy+H11(i)*eps11(i)/2+H22(i)*eps22(i)/2+H33(i)*eps33(i)/2;
    Energy=Energy+H12(i)*eps12(i)+H13(i)*eps13(i)+H23(i)*eps23(i);
end
for i=1:Ln
    Energy=Energy-p3plus*u3(i)*subs(L(i),theta3,h/2);
end
First_Integral=int(Energy,theta1,0,double(a));
PE=int(First_Integral,theta2,0,double(b));
PE=vpa(PE,32);
% Solution of System of Linear Equations
for i=1:Ln
    Der(i)=diff(PE,u10(i));
    Der(Ln+i)=diff(PE,u20(i));
    Der(2*Ln+i)=diff(PE,u30(i));
end
Res=solve(Der);
    
```

Fig. 5. MATLAB module for calculating a total potential energy and solving linear equations.

$$\gamma = \ln(E^+/E^-), \tag{57}$$

where  $E^-$  is the elastic modulus on the bottom surface, whereas the Poisson ratio  $\nu$  is considered to be constant through the thickness [10]. The material parameters are taken to be  $E^+ = 10^7$  Pa and  $\nu = 0.3$ . To compare the results derived with closed-form solutions of elasticity [4,10], the following dimensionless variables are introduced:

$$\bar{u}_1 = G^+ u_1(0, a/2, z)/hp_0, \quad \bar{u}_3 = G^+ u_3(a/2, a/2, z)/hp_0, \quad \bar{\sigma}_{11} = \sigma_{11}(a/2, a/2, z)/p_0, \\ \bar{\sigma}_{12} = \sigma_{12}(0, 0, z)/p_0, \quad \bar{\sigma}_{13} = \sigma_{13}(0, a/2, z)/p_0, \quad \bar{\sigma}_{33} = \sigma_{33}(a/2, a/2, z)/p_0,$$

where  $G^+ = E^+/(2(1 + \nu))$  is the shear modulus on the top surface.

Tables 1 and 2 show results of the convergence study due to increasing the number of SaS. As turned out, the SaS method provides 15 right digits for all basic variables utilizing 13 inner SaS inside the plate body. It should be noted that herein the bottom and top surfaces are not included into a set of SaS because the use of only Chebyshev polynomial nodes allows one to minimize

uniformly the error due to the Lagrange interpolation. Fig. 2 displays distributions of transverse stresses in the thickness direction for the slenderness ratio  $a/h = 1$  employing 11 SaS. These results demonstrate convincingly the high potential of the proposed FG plate formulation because boundary conditions on the bottom and top surfaces of the very thick plate for transverse stresses are satisfied exactly.

Figs. 3–5 list the implementation of the numerical algorithm developed for a homogeneous isotropic plate by means of three MATLAB modules. The first module serves for the computation of Lagrange polynomials (8) and their derivatives (11). The second module provides the calculation of displacements and strains of sampling surfaces (17), (18), (19) and (21). The third one serves for computing the total potential energy (38) and solving the linear algebraic equations (54). This simple implementation emphasizes readability of the MATLAB code and could be useful for the reader for his/her more general implementations.

6.2. Two-phase composite square plate under temperature loading

Here, we study a FG composite plate fabricated by mixing metal and ceramic phases. The simply supported square plate is subjected on the top surface by the sinusoidally distributed temperature whereas the bottom surface is maintained at the reference temperature, that is

$$\Theta^+ = \Theta_0 \sin \frac{\pi x_1}{a} \sin \frac{\pi x_2}{b}, \quad \Theta^- = 0, \tag{58}$$

where  $\Theta_0 = 1$  K,  $T_0 = 293$  K and  $a = b = 1$  m.

It is assumed that the metal phase is aluminum (Al) with material properties [13,14]  $E_m = 7 \times 10^{10}$  Pa,  $\nu_m = 0.3$ ,  $\alpha_m = 23.4 \times 10^{-6}$  1/K,  $k_m = 233$  W/mK,  $\rho_m = 2707$  kg/m<sup>3</sup> and  $c_m = 896$  J/kgK, whereas the material properties of the thermal ceramic barrier (SiC) are  $E_c = 4.27 \times 10^{11}$  Pa,  $\nu_c = 0.17$ ,  $\alpha_c = 4.3 \times 10^{-6}$  1/K,  $k_c = 65$  W/mK,  $\rho_c = 3100$  kg/m<sup>3</sup> and  $c_c = 670$  J/kgK. For evaluating the effective material properties through the thickness of the FG plate, the Mori–Tanaka method [48–51] is invoked

Table 3 Results for a single-layer metal/ceramic square plate with  $a/h = 5$ .

$J_n$	$\bar{u}_1(0.5)$	$\bar{u}_3(0.5)$	$\bar{\sigma}_{11}(0.5)$	$\bar{\sigma}_{12}(0.5)$	$\bar{\sigma}_{13}(0.25)$	$\bar{\sigma}_{33}(0)$	$\bar{\Theta}(0)$	$\bar{q}_1(0)$	$\bar{q}_3(-0.5)$	$\bar{\eta}(0)$
3	-1.2096	4.4213	-3.1907	-6.4775	4.3279	-266.58	0.39780	0.24994	0.59119	86.305
5	-1.2117	4.4198	-4.1612	-6.4890	5.0419	-6.3122	0.39379	0.24742	0.72392	85.605
7	-1.2101	4.4111	-4.1765	-6.4804	4.2085	-8.7894	0.39375	0.24740	0.73125	85.596
9	-1.2101	4.4111	-4.1764	-6.4804	4.2259	-8.6803	0.39375	0.24740	0.73158	85.596
11	-1.2101	4.4111	-4.1764	-6.4804	4.2265	-8.6830	0.39375	0.24740	0.73160	85.596
13	-1.2101	4.4111	-4.1763	-6.4804	4.2264	-8.6829	0.39375	0.24740	0.73160	85.596
15	-1.2101	4.4111	-4.1763	-6.4804	4.2264	-8.6829	0.39375	0.24740	0.73160	85.596
Exact [13]	-1.2101	4.4111	-4.1764	-6.4804	4.2264	-8.6829	0.3938	0.24740	0.7316	

Table 4 Results for a single-layer metal/ceramic square plate with  $a/h = 10$ .

$J_n$	$\bar{u}_1(0.5)$	$\bar{u}_3(0.5)$	$\bar{\sigma}_{11}(0.5)$	$\bar{\sigma}_{12}(0.5)$	$\bar{\sigma}_{13}(0.25)$	$\bar{\sigma}_{33}(0)$	$\bar{\Theta}(0)$	$\bar{q}_1(0)$	$\bar{q}_3(-0.5)$	$\bar{\eta}(0)$
3	-1.2095	3.6353	-3.0497	-6.4773	4.7296	-1259.0	0.42763	0.42763	0.71051	92.759
5	-1.2140	3.6416	-4.1605	-6.5015	5.3713	-13.790	0.42404	0.42404	0.80216	92.184
7	-1.2124	3.6337	-4.1555	-6.4928	4.4563	-9.7655	0.42401	0.42401	0.80723	92.176
9	-1.2124	3.6337	-4.1555	-6.4928	4.4699	-9.1531	0.42401	0.42401	0.80747	92.176
11	-1.2124	3.6337	-4.1555	-6.4928	4.4704	-9.1627	0.42401	0.42401	0.80748	92.176
13	-1.2124	3.6337	-4.1555	-6.4928	4.4703	-9.1622	0.42401	0.42401	0.80748	92.176
15	-1.2124	3.6337	-4.1555	-6.4928	4.4703	-9.1622	0.42401	0.42401	0.80748	92.176
Exact [13]	-1.2124	3.6337	-4.1555	-6.4928	4.4703	-9.1622	0.4240	0.42401	0.8075	

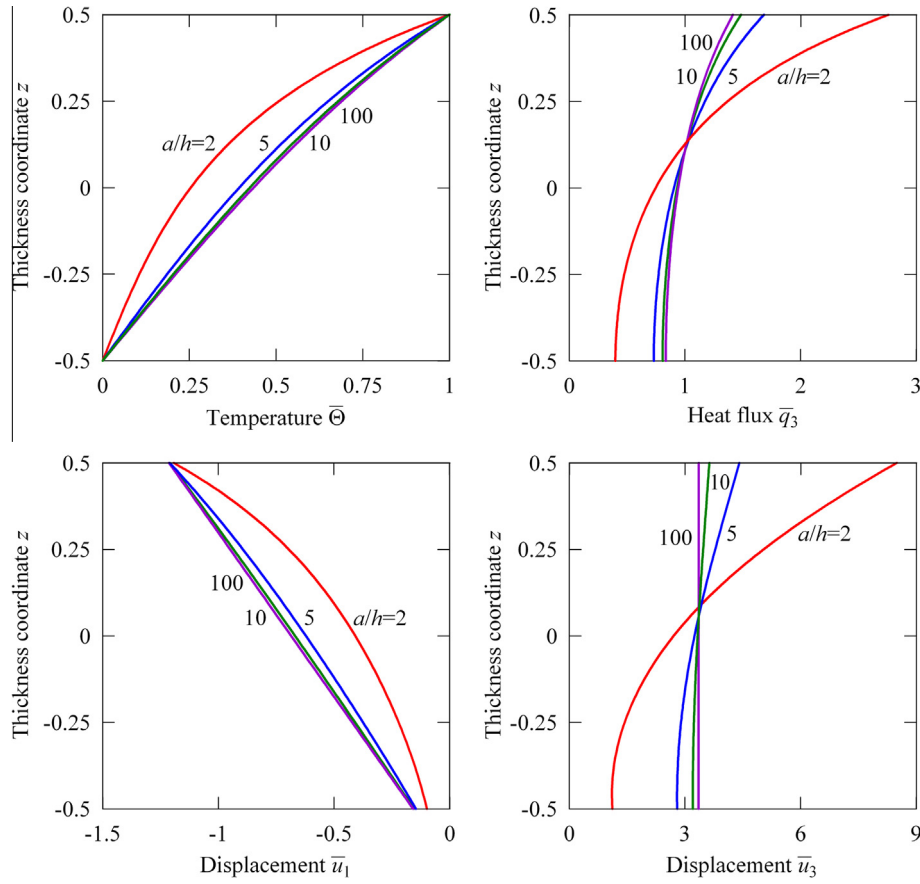


Fig. 6. Through-thickness distributions of temperature, heat flux and displacements for a metal/ceramic FG square plate for  $I_1 = 13$ .

$$\begin{aligned}
 K &= K_m + \frac{V_c(K_c - K_m)}{1 + V_m(K_c - K_m)/(K_m + 4G_m/3)}, \\
 G &= G_m + \frac{V_c(G_c - G_m)}{1 + V_m(G_c - G_m)/(G_m + f_m)}, \quad f_m = \frac{G_m(9K_m + 8G_m)}{6(K_m + 2G_m)}, \\
 k &= k_m + \frac{V_c(k_c - k_m)}{1 + V_m(k_c - k_m)/(3k_m)}, \\
 \alpha &= \alpha_m + \frac{(\alpha_c - \alpha_m)(1/K - 1/K_m)}{1/K_c - 1/K_m}, \\
 c\rho &= c_m\rho_m V_m + c_c\rho_c V_c, \\
 K_m &= \frac{E_m}{3(1 - 2\nu_m)}, \quad K_c = \frac{E_c}{3(1 - 2\nu_c)}, \\
 G_m &= \frac{E_m}{2(1 + \nu_m)}, \quad G_c = \frac{E_c}{2(1 + \nu_c)},
 \end{aligned} \quad (59)$$

where  $K_m$  and  $K_c$  are the bulk moduli of metal and ceramic phases;  $V_m$  and  $V_c$  are the volume fractions of metal and ceramic phases defined as

$$V_m = 1 - V_c, \quad V_c = V_c^- + (V_c^+ - V_c^-)(0.5 + z)^\gamma, \quad z = x_3/h, \quad (60)$$

where  $V_c^-$  and  $V_c^+$  are the volume fractions of the ceramic phase on the bottom and top surfaces;  $\gamma$  is the material gradient index.

To compare results derived with the exact solution of Vel and Batra [13], we accept  $V_c^- = 0$ ,  $V_c^+ = 0.5$  and  $\gamma = 2$ , and introduce dimensionless variables at crucial points

$$\begin{aligned}
 \bar{\Theta} &= \Theta(a/2, a/2, z)/\Theta_0, \quad \bar{q}_3 = -hq_3(0, a/2, z)/k_m\Theta_0, \\
 \bar{q}_3 &= -hq_3(a/2, a/2, z)/k_m\Theta_0, \quad \bar{\eta} = \eta(a/2, a/2, z)/E_m\alpha_m^2\Theta_0, \\
 \bar{u}_1 &= 10u_1(0, a/2, z)/\alpha_m\Theta_0, \quad \bar{u}_3 = 100hu_3(a/2, a/2, z)/a^2\alpha_m\Theta_0, \\
 \bar{\sigma}_{11} &= 10\sigma_{11}(a/2, a/2, z)/E_m\alpha_m\Theta_0, \quad \bar{\sigma}_{12} = 10\sigma_{12}(0, 0, z)/E_m\alpha_m\Theta_0, \\
 \bar{\sigma}_{13} &= 100a\sigma_{13}(0, a/2, z)/hE_m\alpha_m\Theta_0, \quad \bar{\sigma}_{33} = 100a^2\sigma_{33}(a/2, a/2, z)/h^2E_m\alpha_m\Theta_0.
 \end{aligned}$$

Tables 3 and 4 list results of the convergence study utilizing the various number of SaS  $I_1$  inside the plate body. These results demonstrate convincingly the high potential of the developed thermoelastic FG plate formulation. It is important to note that here outer surfaces are included into a set of SaS because of the use of boundary conditions (58). Figs. 6 and 7 show through-thickness distributions of the temperature, heat flux, displacements and stresses for different slenderness ratios  $a/h$  employing 13 SaS throughout the thickness of the FG plate. As can be seen, the boundary conditions for transverse stresses on the bottom and top surfaces are satisfied again exactly.

## 7. Analytical solution for laminated FG plates in cylindrical bending

In this section, we consider a laminated anisotropic FG plate in cylindrical bending subjected to temperature loading. The boundary conditions for the simply supported plate with edges maintained at the reference temperature are written as

$$\sigma_{11}^{(n)} = \sigma_{12}^{(n)} = u_3^{(n)} = \Theta^{(n)} = 0 \text{ at } x_1 = 0 \text{ and } x_1 = a, \quad (61)$$

where  $a$  is the width of the plate. To satisfy boundary conditions, we search for the analytical solution by a method of Fourier series expansion

$$\Theta^{(n)in} = \sum_r \Theta_r^{(n)in} \sin \frac{r\pi x_1}{a}, \quad (62)$$

$$u_1^{(n)in} = \sum_r u_{1r}^{(n)in} \cos \frac{r\pi x_1}{a}, \quad u_2^{(n)in} = \sum_r u_{2r}^{(n)in} \cos \frac{r\pi x_1}{a},$$

$$u_3^{(n)in} = \sum_r u_{3r}^{(n)in} \sin \frac{r\pi x_1}{a}, \quad (63)$$

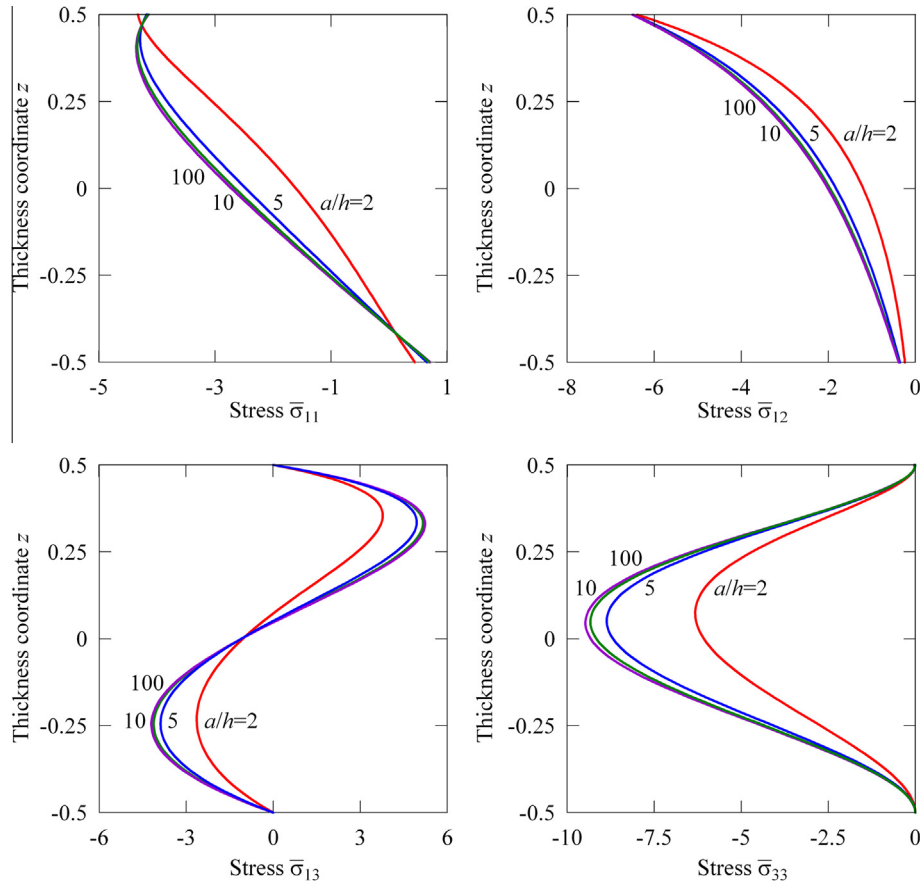


Fig. 7. Through-thickness distributions of stresses for a metal/ceramic FG square plate for  $I_1 = 13$ .

**Table 5**  
Results for an angle-ply FG square plate in cylindrical bending with  $a/h = 2$ .

$I_n$	$\bar{u}_1(0.5)$	$\bar{u}_3(0.5)$	$\bar{\sigma}_{11}(0.5)$	$\bar{\sigma}_{12}(0.5)$	$\bar{\sigma}_{13}(0)$	$\bar{\sigma}_{23}(0)$	$\bar{\sigma}_{33}(0)$	$\bar{\Theta}(-0.125)$	$\bar{q}_3(0)$	$\bar{\eta}(-0.125)$
3	-3.1900	15.778	8.0911	0.57599	-16.254	5.4059	-44.163	0.17315	0.12878	25.423
5	-3.2361	16.213	8.1430	0.57593	-15.268	6.0563	-12.182	0.17634	0.33688	25.797
7	-3.2330	16.191	8.1348	0.57574	-15.585	6.0669	-9.2884	0.17624	0.21846	25.787
9	-3.2330	16.191	8.1359	0.57575	-15.189	6.0481	-10.374	0.17624	0.33462	25.787
11	-3.2330	16.191	8.1360	0.57575	-15.189	6.0482	-10.418	0.17624	0.34058	25.787
13	-3.2330	16.191	8.1360	0.57575	-15.189	6.0482	-10.420	0.17624	0.34087	25.787
					-15.189	6.0482	-10.420	0.17624	0.34088	25.787

**Table 6**  
Results for an angle-ply FG square plate in cylindrical bending with  $a/h = 10$ .

$I_n$	$\bar{u}_1(0.5)$	$\bar{u}_3(0.5)$	$\bar{\sigma}_{11}(0.5)$	$\bar{\sigma}_{12}(0.5)$	$\bar{\sigma}_{13}(0)$	$\bar{\sigma}_{23}(0)$	$\bar{\sigma}_{33}(0)$	$\bar{\Theta}(-0.125)$	$\bar{q}_3(0)$	$\bar{\eta}(-0.125)$
3	-3.5976	10.077	11.033	0.35123	-19.456	2.5751	-126.89	0.67621	0.57070	98.691
5	-3.6562	10.382	11.139	0.36661	-18.896	3.5427	2519.6	0.67613	0.15533	98.669
7	-3.6526	10.364	11.146	0.36569	-19.640	3.4897	-10.309	0.67613	0.58345	98.669
9	-3.6527	10.364	11.147	0.36569	-18.920	3.4729	-18.132	0.67613	0.55498	98.669
11	-3.6527	10.364	11.148	0.36569	-18.905	3.4728	-16.795	0.67613	0.58347	98.669
13	-3.6527	10.364	11.148	0.36569	-18.920	3.4729	-18.132	0.67613	0.58200	98.669
					-18.920	3.4729	-18.054	0.67613	0.58340	98.669
					-18.920	3.4729	-18.132	0.67613	0.58347	98.669
					-18.920	3.4729	-18.129	0.67613	0.58347	98.669
					-18.920	3.4729	-18.132	0.67613	0.58347	98.669

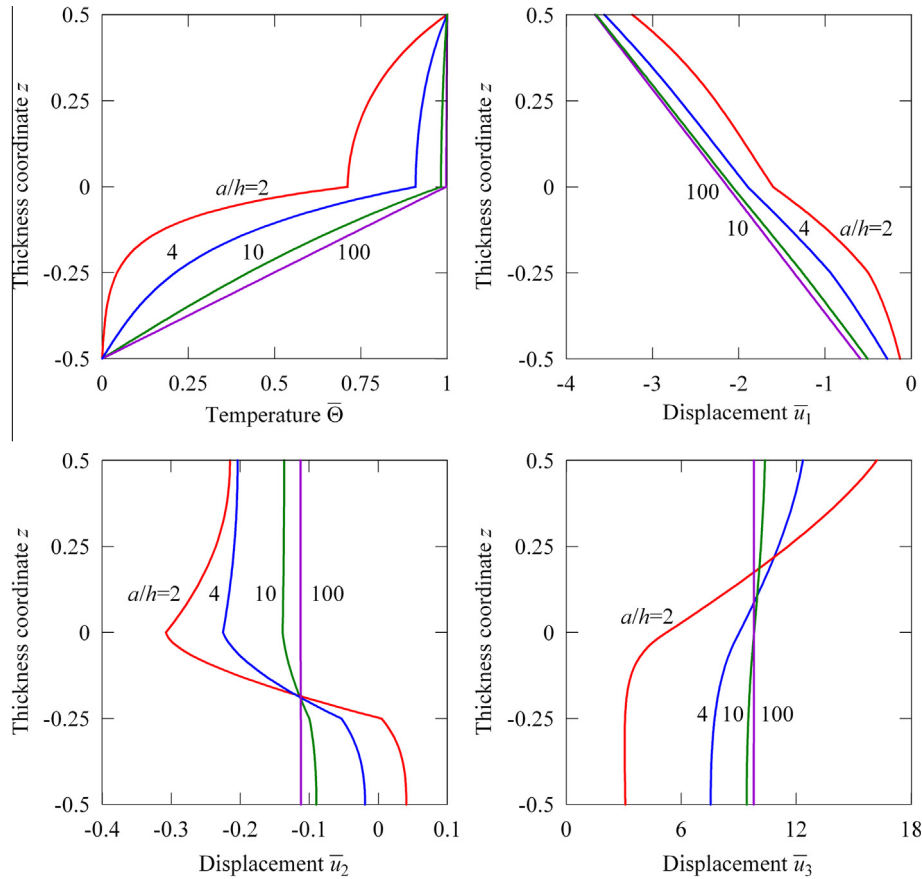


Fig. 8. Through-thickness distributions of the temperature and displacements for an angle-ply FG square plate for  $l_1 = l_2 = l_3 = 13$ .

where  $r$  is the wave number along the  $x_1$ -direction. The external loads are also expanded in Fourier series.

Substituting Fourier series (62) and (63), and Fourier series corresponding to mechanical loading in Eqs. (9), (10), (17)–(19), (21), (25), (28), (33), (38), (45) and (46), one obtains

$$J = \sum_r J_r (\Theta_r^{(n)in}), \quad (64)$$

$$\Pi = \sum_r \Pi_r (u_{ir}^{(n)in}, \Theta_r^{(n)in}). \quad (65)$$

Invoking variational equations (22), (64) and (30), (65), we arrive at two systems of linear algebraic equations

$$\frac{\partial J_r}{\partial \Theta_r^{(n)in}} = 0, \quad (66)$$

$$\frac{\partial \Pi_r}{\partial u_{ir}^{(n)in}} = 0 \quad (67)$$

of orders  $K$  and  $3K$ , respectively, where  $K = \sum_n I_n - N + 1$ . The linear systems (66) and (67) are solved independently by a Gaussian elimination method.

The described algorithm was performed with the Symbolic Math Toolbox, which incorporates symbolic computations into the numeric environment of MATLAB. This gives the possibility to derive analytical solutions for thermoelastic laminated anisotropic FG plates in cylindrical bending with a specified accuracy.

As a numerical example, we study a two-layer square plate [45/–45] composed of the graphite/epoxy composite and covered with the metal/ceramic barrier on its top surface. Thus, a three-layer plate with the stacking sequence [45/–45/FGM] and

ply thicknesses [0.25h/0.25h/0.5h] is considered. The mechanical properties of the graphite/epoxy composite are taken as follows:  $E_L = E_0$ ,  $E_T = E_0/10$ ,  $G_{LT} = E_0/20$ ,  $G_{TT} = E_0/50$ ,  $\nu_{LT} = \nu_{TT} = 0.25$ ,  $\alpha_L = \alpha_0$ ,  $\alpha_T = 7.2\alpha_0$ ,  $k_L = 100k_0$ ,  $k_T = k_0$ ,  $\rho = 1800 \text{ kg/m}^3$  and  $c_v = 900 \text{ J/kgK}$ , where  $E_0 = 2 \times 10^{11} \text{ Pa}$ ,  $\alpha_0 = 5 \times 10^{-6} \text{ 1/K}$  and  $k_0 = 0.5 \text{ W/mK}$ . The mechanical properties of the metal/ceramic composite are given in Section 6.2. For evaluating the effective material properties through the thickness of the metal/ceramic barrier, the Mori-Tanaka scheme (59) is utilized with a specific distribution of the volume fraction of the ceramic phase

$$V_c = V_c^- + (V_c^+ - V_c^-)(2z)^\gamma, \quad 0 \leq z \leq 0.5, \quad z = x_3/h, \\ V_c^- = 0, \quad V_c^+ = 0.5, \quad \gamma = 2. \quad (68)$$

It is assumed that the plate is loaded on the top surface by the sinusoidally distributed temperature whereas the bottom surface is maintained at the reference temperature, that is

$$\Theta^+ = \Theta_0 \sin \frac{\pi x_1}{a}, \quad \Theta^- = 0, \quad (69)$$

where  $a = 1 \text{ m}$ ,  $\Theta_0 = 1 \text{ K}$  and  $T_0 = 293 \text{ K}$ . To analyze derived results efficiently, we introduce the following dimensionless variables at crucial points:

$$\bar{\Theta} = \Theta(a/2, z)/\Theta_0, \quad \bar{q}_3 = -aq_3(a/2, z)/k_m \Theta_0, \\ \bar{\eta} = \eta(a/2, z)/E_m \alpha_m^2 \Theta_0, \\ \bar{u}_x = 10u_x(0, z)/a \alpha_m \Theta_0, \quad \bar{u}_3 = 100hu_3(a/2, z)/a^2 \alpha_m \Theta_0, \\ \bar{\sigma}_{11} = 10\sigma_{11}(a/2, z)/E_m \alpha_m \Theta_0, \quad \bar{\sigma}_{12} = 10\sigma_{12}(a/2, z)/E_m \alpha_m \Theta_0, \\ \bar{\sigma}_{z3} = 100a\sigma_{z3}(0, z)/hE_m \alpha_m \Theta_0, \\ \bar{\sigma}_{33} = 100a^2\sigma_{33}(a/2, z)/h^2E_m \alpha_m \Theta_0.$$

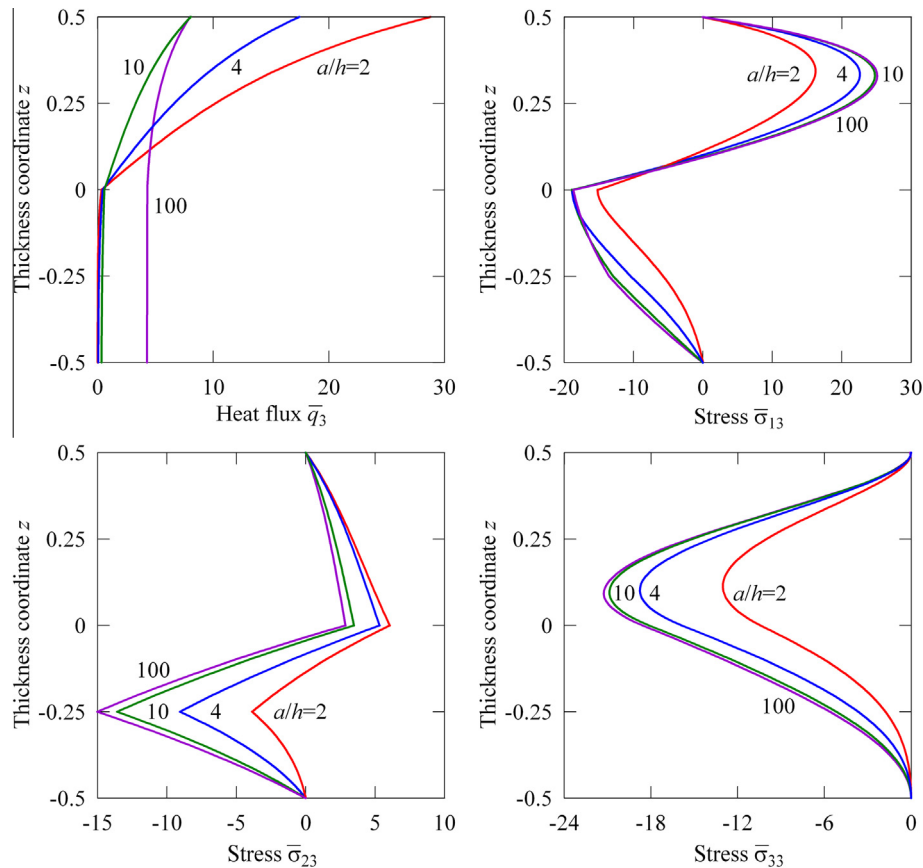


Fig. 9. Through-thickness distributions of the heat flux and transverse stresses for an angle-ply FG square plate in cylindrical bending for  $I_1 = I_2 = I_3 = 13$ .

The data listed in Tables 5 and 6 show that the SaS method permits the derivation of analytical solutions for thick angle-ply FG plates with a prescribed accuracy using the sufficiently large number of SaS. Note that transverse components of the heat flux and stresses are calculated at the interface between the plate and the metal/ceramic barrier. Figs. 8 and 9 display through-thickness distributions of the temperature, displacements, heat flux and stresses for different slenderness ratio  $a/h$  by choosing 13 SaS for each layer. As can be seen, the boundary conditions for transverse stresses on the bottom and top surfaces and the continuity conditions for a heat flux and transverse stresses at both interfaces are satisfied again exactly.

## 8. Conclusions

An efficient method of solving the steady-state problems of 3D thermoelasticity for laminated FG plates has been proposed. It is based on a new method of SaS located at Chebyshev polynomial nodes throughout the layers. This permits one to minimize uniformly the error due to Lagrange interpolation. The thermal stress formulation for laminated orthotropic and anisotropic FG plates is based on 3D constitutive equations and gives the possibility to obtain the analytical solutions of thermoelasticity for thick and thin laminated FG plates with a prescribed accuracy by using the sufficient number of SaS.

## Acknowledgement

This work was supported by Russian Ministry of Education and Science under Grant No 9.137.2014/K and by Russian Foundation for Basic Research under Grant No 13–01–00155.

## References

- [1] Koizumi M. FGM activities in Japan. *Composites Part B* 1997;28:1–4.
- [2] Birman V, Byrd LW. Modeling and analysis of functionally graded materials and structures. *Appl Mech Rev* 2007;60:195–216.
- [3] Jha DK, Kant T, Singh RK. A critical review of recent research on functionally graded plates. *Compos Struct* 2013;96:833–49.
- [4] Vlasov BF. On the bending of a rectangular thick plate. *Vestnik Moskov Univ Ser Mat Mekh* 1957;N2:25–31 (in Russian).
- [5] Pagano NJ. Exact solutions for rectangular bidirectional composites and sandwich plates. *J Compos Mater* 1970;4:20–34.
- [6] Alibeigloo A. Exact solution for thermo-elastic response of functionally graded rectangular plates. *Compos Struct* 2010;92:113–21.
- [7] Alibeigloo A, Liew KM. Thermoelastic analysis of functionally graded carbon nanotube-reinforced composite plate using theory of elasticity. *Compos Struct* 2013;106:873–81.
- [8] Cheng ZQ, Batra RC. Three-dimensional thermoelastic deformations of a functionally graded elliptic plate. *Composites Part B* 2000;31:97–106.
- [9] Reddy JN, Cheng ZQ. Three-dimensional thermomechanical deformations of functionally graded rectangular plates. *Eur J Mech A/Solids* 2001;20:841–55.
- [10] Kashtalyan M. Three-dimensional elasticity solution for bending of functionally graded rectangular plates. *Eur J Mech A/Solids* 2004;23:853–64.
- [11] Woodward B, Kashtalyan M. Three-dimensional elasticity solution for bending of transversely isotropic functionally graded plates. *Eur J Mech A/Solids* 2011;30:705–18.
- [12] Plevako VP. On the theory of elasticity of inhomogeneous media. *J Appl Math Mech* 1971;35:806–13.
- [13] Vel SS, Batra RC. Exact solution for thermoelastic deformations of functionally graded thick rectangular plates. *AIAA J* 2002;40:1421–33.
- [14] Vel SS, Batra RC. Three-dimensional analysis of transient thermal stresses in functionally graded plates. *Int J Solids Struct* 2003;40:7181–96.
- [15] Ootao Y. Transient thermoelastic analysis for a multilayered thick strip with piecewise exponential nonhomogeneity. *Composites Part B* 2011;42:973–81.
- [16] Ootao Y, Ishihara M. Three-dimensional solution for transient thermoelastic problem of a functionally graded rectangular plate with piecewise exponential law. *Compos Struct* 2013;106:672–80.
- [17] Ootao Y, Tanigawa Y. Three-dimensional solution for transient thermal stresses of an orthotropic functionally graded rectangular plate. *Compos Struct* 2007;80:10–20.

- [18] Altenbach H, Eremeyev VA. Direct approach-based analysis of plates composed of functionally graded materials. *Arch Appl Mech* 2008;78:775–94.
- [19] Birsan M, Altenbach H, Sadowski T, Eremeyev VA, Pietras D. Deformation analysis of functionally graded beams by the direct approach. *Composites Part B* 2012;43:1315–28.
- [20] Zhilin PA. Mechanics of deformable directed surfaces. *Int J Solids Struct* 1976;12:635–48.
- [21] Altenbach H, Naumenko K, Zhilin PA. A direct approach to the formulation of constitutive equations for rods and shells. In: Pietraszkiewicz W, Szymczak C, editors. *Shell structures: theory and applications*. London: Taylor and Francis; 2006. p. 87–90.
- [22] Kulikov GM, Plotnikova SV. Heat conduction analysis of laminated shells by a sampling surfaces method. *Mech Res Commun* 2014;55:59–65.
- [23] Kulikov GM, Plotnikova SV. 3D exact thermoelastic analysis of laminated composite shells via sampling surfaces method. *Compos Struct* 2014;115:120–30.
- [24] Kulikov GM, Plotnikova SV. Three-dimensional thermal stress analysis of laminated composite plates with general layups by a sampling surfaces method. *Eur J Mech A/Solids* 2015;49:214–26.
- [25] Kulikov GM, Plotnikova SV. A new approach to three-dimensional exact solutions for functionally graded piezoelectric laminated plates. *Compos Struct* 2013;106:33–46.
- [26] Kulikov GM, Plotnikova SV. Exact electroelastic analysis of functionally graded piezoelectric shells. *Int J Solids Struct* 2014;51:13–25.
- [27] Kulikov GM, Plotnikova SV. Exact 3D stress analysis of laminated composite plates by sampling surfaces method. *Compos Struct* 2012;94:3654–63.
- [28] Kulikov GM, Plotnikova SV. Advanced formulation for laminated composite shells: 3D stress analysis and rigid-body motions. *Compos Struct* 2013;95:236–46.
- [29] Runge C. Über empirische Funktionen und die Interpolation zwischen äquidistanten Ordinaten. *Z Math Physik* 1901;46:224–43.
- [30] Burden RL, Faires JD. *Numerical analysis*. 9th ed. Boston: Brooks/Cole, Cengage Learning; 2010.
- [31] Carrera E. Theories and finite elements for multilayered, anisotropic, composite plates and shells. *Arch Comput Methods Eng* 2002;9:1–60.
- [32] Grigolyuk EI, Chulkov PP. On the theory of multilayer shells. In: *Contributions to the theory of aircraft structures*. Delft: University Press; 1972. p. 171–83.
- [33] Librescu L. Improved linear theory of elastic anisotropic multilayered shells. Part 1. *Mech Compos Mater* 1975;11:885–96.
- [34] Epstein M, Glockner PG. Nonlinear analysis of multilayered shells. *Int J Solids Struct* 1977;13:1081–9.
- [35] Grigolyuk EI, Kulikov GM. Toward a theory of elastic laminated anisotropic shells. *Sov. Phys. Doklady* 1984;29:344–5.
- [36] Reddy JN. On the generalization of displacement-based laminate theories. *Appl Mech Rev* 1989;42:S213–22.
- [37] Cho KN, Bert CW, Striz AG. Free vibrations of laminated rectangular plates analyzed by higher order individual-layer theory. *J Sound Vib* 1991;145:429–42.
- [38] Reddy JN. *Mechanics of laminated composite plates and shells: theory and analysis*. 2nd ed. Boca Raton: CRC Press; 2004.
- [39] Carrera E. Theories and finite elements for multilayered plates and shells: a unified compact formulation with numerical assessment and benchmarking. *Arch Comput Methods Eng* 2003;10:215–96.
- [40] Cinefra M, Carrera E, Brischetto S, Belouettar S. Thermo-mechanical analysis of functionally graded shells. *J Therm Stress* 2010;33:942–63.
- [41] Brischetto S, Carrera E. Heat conduction and thermal analysis in multilayered plates and shells. *Mech Res Commun* 2011;38:449–55.
- [42] Kulikov GM. Refined global approximation theory of multilayered plates and shells. *J Eng Mech* 2001;127:119–25.
- [43] Kulikov GM, Carrera E. Finite deformation higher-order shell models and rigid-body motions. *Int J Solids Struct* 2008;45:3153–72.
- [44] Kulikov GM, Plotnikova SV. Solution of statics problems for a three-dimensional elastic shell. *Doklady Phys* 2011;56:448–51.
- [45] Kulikov GM, Plotnikova SV. Non-linear strain–displacement equations exactly representing large rigid-body motions. Part II. Enhanced finite element technique. *Comput Methods Appl Mech Eng* 2006;195:2209–30.
- [46] Kulikov GM, Plotnikova SV. Non-linear exact geometry 12-node solid-shell element with three translational degrees of freedom per node. *Int J Numer Methods Eng* 2011;88:1363–89.
- [47] Kovalenko AD. *Thermoelasticity. Basic theory and applications*. Groningen: Wolters-Noordhoff; 1969.
- [48] Mori T, Tanaka K. Average stress in matrix and average elastic energy of materials with misfitting inclusions. *Acta Metall* 1973;21:571–4.
- [49] Benveniste Y. A new approach to the application of Mori–Tanaka’s theory in composite materials. *Mech Mater* 1987;6:147–57.
- [50] Hatta H, Taya M. Effective thermal conductivity of a misoriented short fiber composite. *J Appl Phys* 1985;58:2478–86.
- [51] Rosen BW, Hashin Z. Effective thermal expansion coefficients and specific heats of composite materials. *Int J Eng Sci* 1970;8:157–73.